

Full paper

Optimized hetero-interfaces by tuning 2D SnS₂ thickness in Bi₂Te_{2.7}Se_{0.3}/SnS₂ nanocomposites to enhance thermoelectric performance



Shuankui Li^a, Xuerui Liu^a, Yidong Liu^a, Fusheng Liu^b, Jun Luo^c, Feng Pan^{a,*}

^a School of Advanced Materials, Peking University Shenzhen Graduate School, Shenzhen 518055, China

^b College of Materials Science and Engineering, Shenzhen University and Shenzhen Key Laboratory of Special Functional Materials, Shenzhen 518060, China

^c School of Materials Science and Engineering, Shanghai University, Shanghai 200444, China

ARTICLE INFO

Keywords:

Thermoelectric materials
Bi₂Te₃ nanostructure
Heterogeneous
Energy filtering
Phonon scattering

ABSTRACT

Tuning the electron and phonon transport properties of thermoelectric materials to partially decouple electrical conductivity, Seebeck coefficient and thermal conductivity is the core issue to improve the conversion efficiency. Herein, Bi₂Te_{2.7}Se_{0.3}/SnS₂ nanocomposites with a unique hetero-structure that the 2D atomically thin SnS₂ nanosheets (2–15 nm) homogeneously assembled on BTS grain boundaries have been successfully synthesized to explore the size-dependent electron and phonon regulating effects. The atomically thin Bi₂Te_{2.7}Se_{0.3}/SnS₂ interfaces allow for effective phonon scattering and decreased thermal conductivity, while the energy filtering effect increase the power factor, resulting an improved figure of merit (ZT). By controlling the thickness of the interfaces SnS₂ layers, simultaneously optimized the electron transporting and phonon scattering properties has been achieved, a high ZT = 0.93 at 450 K is obtained. The designed Bi₂Te_{2.7}Se_{0.3}/SnS₂ nanocomposites give us opportunities to systematically study the size-dependent electron tuning effect (energy filtering effect) and phonon scattering (classical size effect), which finally give rise to the enhancement of ZT.

1. Introduction

Thermoelectric (TE) materials for direct conversion between electricity and waste heat has been attracted great attention because the worlds energy consumption wasted in the form of heat is more than 50% [1–3]. Tuning the electron and phonon transport properties of thermoelectric materials to partially decouple electrical conductivity (σ), Seebeck coefficient (S) and thermal conductivity (κ) is the core issue for improve the conversion efficiency [4–6]. The design of nanocomposites thermoelectric materials has been considered an effective way to solve the above problems, and the hetero-interface could be designed to scatter phonons more effectively than electrons, resulting enhanced ZT [7,8]. The goals of designing nanocomposite thermoelectric materials are introducing hetero-interfaces specially chosen to: 1) reduce the thermal conductivity more than the electrical conductivity by interface scattering, and 2) tune the electron transport property increasing S (for example, by carrier-energy filtering or by quantum confinement) more than decreasing the electrical conductivity, thereby resulting the increased power factor, with both goals helping to increase ZT [9,10]. Unfortunately, in the recent reported nanocomposites, the enhancement of ZT mostly comes from the reduction in lattice thermal conductivity because the hetero-interfaces

could potentially hinder electron transport. Therefore, design the hetero-interface within a nanocomposite which could simultaneously optimize the electron and phonon transport is highly desirable and central theme for high zT.

In nanocomposite, manipulating of the electronic properties can be mainly resulted from the energy filtering effect at the hetero-interfaces. The energy barriers at the hetero-interfaces would be expected to filter out low-energy carriers so that the average energy of the carriers is moved further from the Fermi level, resulting an enhanced S , which is the so-called energy filtering effect [11–13]. The energy filtering effect is related to the energy barrier height determined by the band structure and the size-dependent energy barrier width. It is well known that for the energy barrier height, the nearly zero bands offset has a minimized interference to electron transport, which has been confirmed by previous reports [11,14–16]. For the energy barrier width, once it is comparable to or smaller than the carriers mean free path and/or coherence length, the quantum confinement effect could occur to enhance the Seebeck coefficient due to the sharp transitions of the density of states (DOS) near the Fermi level [17–19]. This effect is crucial to the nanocomposite thermoelectric materials, but is very difficult to be explored experimentally because the precise tuning to the energy barrier height and width is usually hard [20,21]. Herein,

* Corresponding author.

E-mail address: panfeng@pkusz.edu.cn (F. Pan).

designing nanocomposites with the controllable hetero-interfaces by introducing the 2D transition-metal dichalcogenide (TMD) nanosheets to nano $\text{Bi}_2\text{Te}_{2.7}\text{Se}_{0.3}$ (BTS) matrix as a novel thought and method is proposed to explore the electron and phonon filtering effect. This work reports an interesting exploration to the high-performance TE materials by designing and fabricating the $\text{Bi}_2\text{Te}_3/2\text{D}$ TMD nanosheets nanocomposites with the optimum hetero-structure that SnS_2 layers with proper thickness assembled at the interface of nanograins to tuning the electron and phonon transport properties.

Inspired by the aforementioned concepts, we explored the size-dependent electron and phonon regulating effects for enhancing thermoelectric performance by optimizing heterostructure through tuning thickness of 2D atomically thin SnS_2 nanosheets, which were distributed on BTS grain boundaries to generate $\text{Bi}_2\text{Te}_{2.7}\text{Se}_{0.3}/\text{SnS}_2$ (BTS/SS) nanocomposites. In such nanocomposites, the SnS_2 nanosheets (2–15 nm) are homogeneously distributed on BTS grain boundaries to produce a 3D- SnS_2 network wrapping BTS matrix architecture. The well-designed 3D SnS_2 network structure is found to be effective in improving ZT of nanocomposite by reducing the κ_{lat} while enhancing the power factor $S^2\sigma$. The ZT value of the BTS/SS nanocomposites is 0.93 at 450 K (the thickness of SnS_2 layer is only about 2 nm, and the content is about 1.47 vol%), 2.3 times higher than that of pure BTS. We also demonstrate that the electronic properties as well as the grain boundary thermal resistivity exhibit a critical SnS_2 thickness dependence, suggesting the size-dependent regulating effect of 2D hetero-interfaces. This work provides sufficient versatility to harness the key benefits of nanocomposites by selecting TMD with appropriate Fermi levels and allowing a precise control of nanosheet thickness and volume fraction.

2. Experimental section

2.1. Materials

TeO_2 powder (99.999%), SeO_2 powder (99.999%), $\text{Bi}(\text{NO}_3)_3 \cdot 5\text{H}_2\text{O}$ (99.999%), NaOH (99.999%), Vitamin C, $\text{SnCl}_4 \cdot 5\text{H}_2\text{O}$ (99.999%), thiourea, polyvinylpyrrolidone (PVP, average mol. wt. 40000), ethylene glycol, acetone, ethanol and HCl were purchased from the Shanghai Reagent Company. All the chemicals were used as obtained without further purification.

2.2. Synthesis of BTS nanosheet

BTS nanosheets were synthesized through a simple solution-based synthetic strategy as described in our previous report after some modifications. For the synthesis of the BTS nanosheet, the Bi and Te precursor solutions were separately prepared. All syntheses were carried out under Ar atmosphere using standard Schlenk line techniques. The Te precursor solution was prepared by adding 2.4 g of NaOH, 1.74 g of TeO_2 , 0.13 g of SeO_2 and 60 mL of ethylene glycol to a three-neck flask under magnetic stirring until all of them dissolved. The Bi precursor solution was prepared by dissolving 3.88 g of $\text{Bi}(\text{NO}_3)_3 \cdot 5\text{H}_2\text{O}$ and 0.528 g of Vitamin C in 20 mL of ethylene glycol. Then, the three-neck flask is heated to 160 °C and then the as-prepared Bi precursor solution is injected into the above solution. After reaction for another 2 h, the products were collected by filtration, successively washed several times with deionized water and absolute ethanol, and dried at 60 °C for 24 h.

2.3. Synthesis of SnS_2 nanosheets

For the synthesis of SnS_2 nanosheets, 0.40 g of $\text{SnCl}_4 \cdot 5\text{H}_2\text{O}$, 0.228 g of thiourea and an amount of PVP (SnS_2 -t1, without PVP; SnS_2 -t2, 0.10 g of PVP; SnS_2 -t3, 0.40 g of P; SnS_2 -t4, 0.60 g of PVP) dissolve in 40 mL of deionized water under magnetic stirring. The resulting solution was transferred into a Teflon-lined stainless autoclave

(50 mL capacity), followed by solvothermal treatment at 180 °C for 18 h. The products were collected by filtration, successively washed several times with deionized water and absolute ethanol, and dried at 60 °C for 24 h. The thickness of SnS_2 nanosheets could be regulated by the amount of PVP.

The as prepared BTS nanosheets and SnS_2 nanosheets dispersed separately in ethanol. After sonicated at a low power sonic bath for 2 h, the resulting solution was mixed under magnetic stirring to synthesis the BTS/SS hybrids. After sonicate and stirring for another 2 h, the products were collected by filtration, successively washed several times with deionized water and absolute ethanol, and dried at 60 °C for 24 h.

2.4. Characterisation

X-ray diffraction (XRD) was performed on a Bruker D8 Advance powder X-ray diffractometer; field-emission scanning electron microscopy (SEM) on a Zeiss SUPRA-55; transmission electron microscopy (TEM) on a JEOL-3200 instrument. X-ray photoelectron spectra (XPS) were acquired on Thermo Fisher ESCALAB 250X surface analysis system equipped with a monochromatized Al anode X-ray source (X-ray photoelectron spectroscopy, XPS, $h\nu = 1486.6$ eV).

2.5. Thermoelectric measurements

The dry powders pressed into pellets by spark plasma sintering (SPS) at 623 K for 5 min under vacuum with a uniaxial pressure of 50 MPa. The pellets were cylinders with 10 mm in diameter and 12 mm in height. The disk with thickness of around 2 mm was cut from the sintered pellets to measure the thermal conductivity, and a cuboid about 3 mm × 3 mm × 10 mm was cut to measure the σ and S . The electrical conductivity and Seebeck coefficient were measured using ULVAC ZEM-3 within the temperature range 300–480 K. The total thermal conductivity (κ_{tot}) was calculated through $\kappa_{\text{tot}} = DC_p\rho$, where D , C_p , and ρ are the thermal diffusivity coefficient, specific heat capacity, and density, respectively. The thermal diffusivity coefficient was measured by a laser flash apparatus using Netzsch LFA 457 from 300 to 480 K, and the specific heat (C_p) was tested by a differential scanning calorimeter (Mettler DSC1), and the density (ρ) was calculated by using the mass and dimensions of the pellet. The bulk sample with length ~ 10 mm, width ~ 2.5 mm and thickness ~ 1 mm was used to measure the carrier density and carrier mobility by physical properties measurement system (PPMS, Quantum Design).

3. Results and discussion

SnS_2 is one of the n-type semiconductors with band gap of 2.24 eV that have a layered CdI_2 -type structure with a hexagonal unit cell, which has a sandwich structure that consists of covalently bonded S–Sn–S trilayers extend in a and b-directions, and a van der Waals interaction in the c-direction [22–24]. As for the SnS_2 , the (001) surface is the most stable, which will lead to the anisotropy growth with exposed (001) facets. If we introduce additives with stronger absorption on the (001) surface during the synthesis process to stabilize (001) surface, and thinner (001) sheets or plates can be obtained. In this work, we used polyvinylpyrrolidone (PVP) as additives to adjust the thickness of SnS_2 nanosheets. The XRD patterns (Fig. S1) of the as-prepared SnS_2 nanosheets exhibit prominent peaks in agreement with the SnS_2 phase. The SEM and TEM reveal that the formation of SnS_2 nanosheets (Fig. S2). As the PVP content increased, the thickness of SnS_2 nanosheet is decreased from 15 nm to about 2 nm. Thus, four types of SnS_2 nanosheets with different thickness (SnS_2 -t1 (~ 15 nm), SnS_2 -t2 (~ 6 nm), SnS_2 -t3 (~ 4 nm), and SnS_2 -t4 (~ 2 nm)) were prepared to construct the BTS/SS nanocomposites.

BTS is a type of anisotropic layered material, which preferentially grow into 2D structures extend in a and b-directions due to the weak van der Waals interaction along the c-axis. The BTS nanosheets were

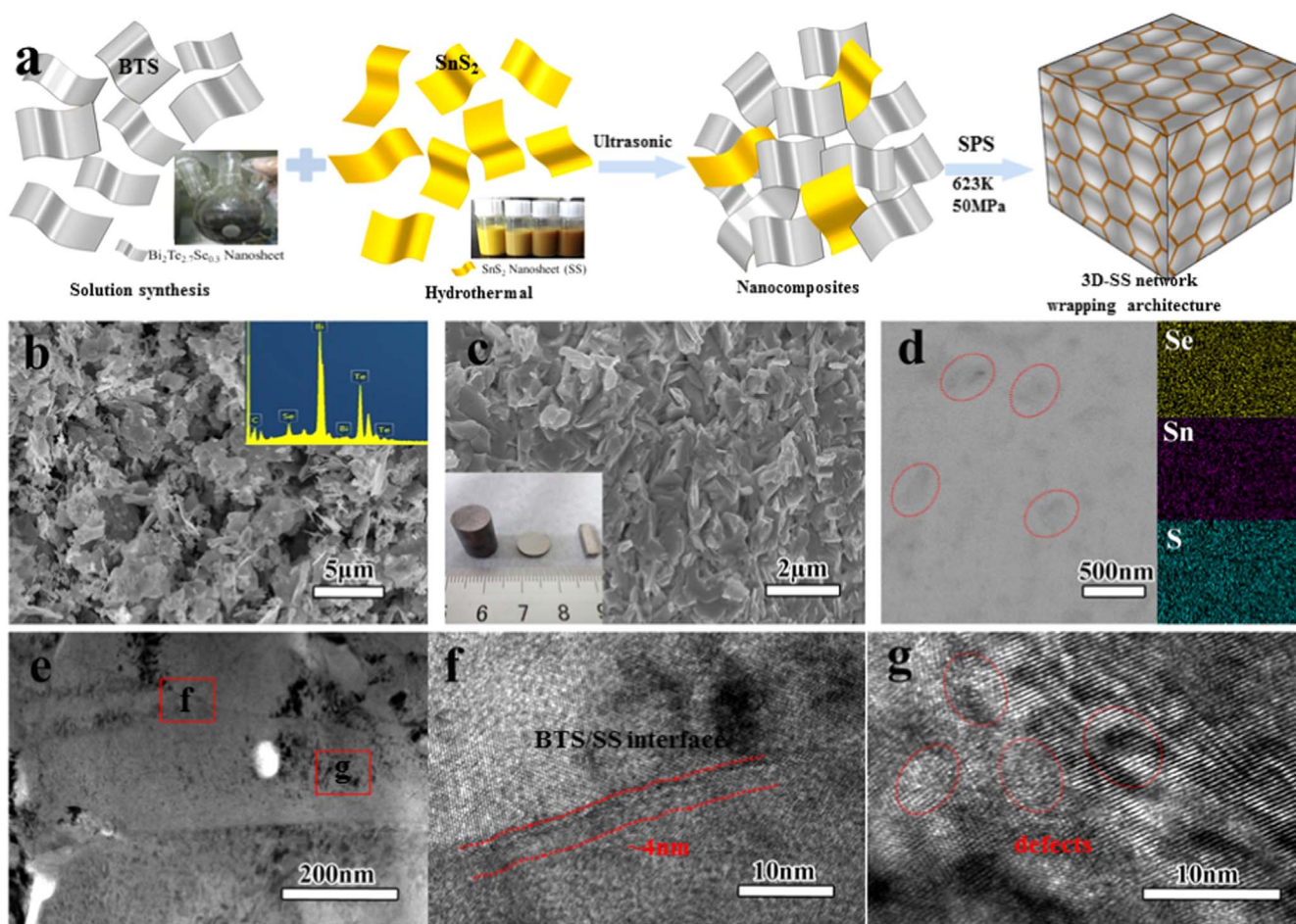


Fig. 1. (a) A schematic synthesis process of BTS/SS nanocomposites. (b) FE-SEM image (the inset is the corresponding EDS pattern) of BTS nanosheet. (c) FE-SEM images of the fractured surfaces of BTS/SS nanocomposites. (d) BSE and corresponding EDS mapping images. The TEM image of the BTS/SS3 bulk, (e) low-magnification TEM image and (f) HRTEM image showing the SnS_2 nanosheet about 4 nm thickness, (g) HRTEM image region d.

synthesized through a simple solution-based process. The SEM and TEM images reveal the formation of irregular nanoplatelets with lateral dimensions of more than $5 \mu\text{m}$ and a thickness of a few tens of nanometres (Fig. 1b. and Fig. S3). As mentioned above, the preferential growth into 2D structures is determined intrinsically by the anisotropic Bi-Te atom layer structure of orthorhombic BT [25]. The energy-dispersive X-ray spectrum (EDS, the inset in Fig. 1b) exhibits strong Bi, Te and Se peaks, and the atomic ratio corresponds to the 2: 2.7: 0.3 stoichiometry. The as-prepared SnS_2 and BTS nanosheets were ultrasonically dispersed in ethanol and mixed under magnetic stirring to synthesize the BTS/SS nanocomposites. The synthesis process is schematically shown in Fig. 1a.

The BTS/SS nanocomposites were sintered by spark plasma sintering in graphite die to fabricate the bulk. The as-obtained BTS/SS nanocomposites were spark plasma sintered (SPSed) at 623 K for 5 min under vacuum with a uniaxial pressure of 50 MPa into a $\phi 10$ mm cylinder with 12 mm in height. It is found that the XRD pattern of the SPSed bulk sample matches well with the standard peaks of BT. No diffraction peaks of SnS_2 are detected in the BTS/SS nanocomposites sample owing to its low content. The diffraction peaks become weaker after SPSed, exhibiting a significant randomness of the tiny size grains, which agrees with the SEM results (Fig. 1c and Fig. S4). Relatively fine grains about 50–100 nm are obtained in the SPSed samples, since the SPS method has an advantage for preparing nanostructured bulk materials owing to its very fast heating and cooling rates. In our experiments, as-prepared BTS/SS nanocomposites can be densified in a short period by SPS, which could prevent unwanted grain growth especially for SnS_2 nanosheets with thin thickness and crucial to the

formation of the 3D- SnS_2 network wrapping architecture. The BSE and corresponding EDS mapping images confirmed that SnS_2 nanosheets are homogeneously distributed throughout the bulk sample without aggregation and growth at SPS process (Fig. 1d). This result could be attributed to the thin thickness of both the SnS_2 nanosheets (2–10 nm) and BTS matrix, which ensures the homogeneous distribution of SnS_2 nanosheets under the sonicated condition. Moreover, as a stable compound, SnS_2 reveals a high decomposition temperature (about 873°C) significantly higher than the SPS temperature, which guaranteed the SnS_2 nanosheets without decomposition at SPS process. XPS analysis reveals the Sn 3d peaks (Sn 3d_{5/2} at 486.8 eV and Sn 3d_{3/2} at 495.4 eV) and S 2p (S2p_{3/2} at 161.83 eV and S2p_{1/2} at 164.2 eV) peaks agree well with the reference data of SnS_2 , as shown in Fig. S5 [26,27]. The XPS spectra of the BTS/SS nanocomposites show no obvious change after SPS process, which also confirmed the existence of SnS_2 nanosheets in the SPSed bulk samples. Therefore, the BTS/SS composites, in which the 2D atomically thin SnS_2 nanosheets (2–10 nm) are homogeneously distributed on BTS grain boundaries to produce a 3D- SnS_2 network, have been successfully fabricated.

TEM investigation has been employed to analyze the structural characteristics of the BTS/SS nanocomposites pellets. Both SEM and TEM images (Fig. 1 and Fig. S6) reveal the random stacking of nano grains with clear grain boundaries. The low-magnification TEM image (Fig. 1e) reveals that the matrix particles are distinctly and equably separated by SnS_2 nanosheets, which agree with the above discussion. The HRTEM image of the interface (BTS/SS-3) further demonstrates that the nano grains are separated by SnS_2 nanosheets with 4 nm thickness, which coincides with the thickness of initial SnS_2 na-

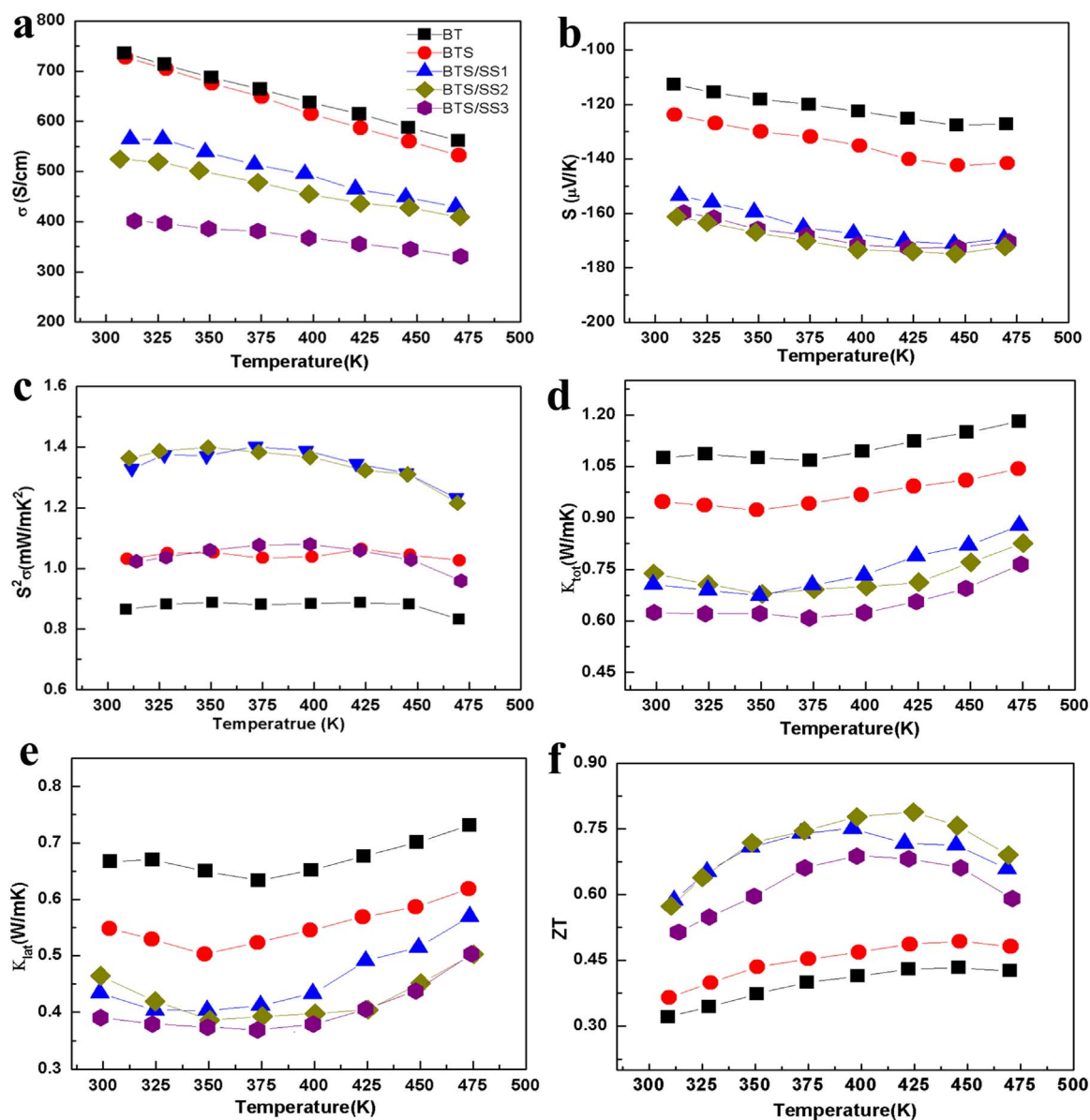


Fig. 2. Thermoelectric properties of the BTS/SS nanocomposites with different SnS₂ contents. (a) electrical conductivity (σ), (b) Seebeck coefficient (S), (c) power factor ($S^2\sigma$), (d) total thermal conductivity (κ_{tot}), (e) lattice thermal conductivity (κ_{latt}) and (f) thermoelectric figure of merit ZT .

nosheets. Moreover, it is found in some regions (Fig. S6), 2–3 layers of SnS₂ nanosheets stacked on the interface, which caused the average thickness of the SnS₂ layers on the grain boundary slightly larger than the thickness of SnS₂ layers on other places. Furthermore, there are some atomic scale distortions and nanoscale distorted regions existence in the SPSe pellets (Fig. 1f). From the above analysis, it can be concluded that BTS/SS nanocomposites is experimentally established, in which 2D atomically thin SnS₂ nanosheets are homogeneously distributed on BTS grain boundaries to produce a 3D-SnS₂ network to wrap BTS architecture.

The thermoelectric properties of the BTS/SS nanocomposites were measured in the temperature range of 300–480 K along the out-of-plane direction, as shown in Fig. 2. A series of BTS/SS nanocomposites with different SnS₂ nanosheet (SnS₂-t3, 4 nm) concentrations (BTS/SS1, 0.97 vol%; BTS/SS2, 1.47 vol%; BTS/SS3, 1.96 vol%) were prepared and analyzed to determine the optimal SnS₂ nanosheet content. SnS₂-free BT and BTS exhibited relatively high electrical conductivities (728–532 S/cm) with a typical degenerated semiconductor behavior, which is comparable to the reported BT-based nanomaterials [28–30]. As illustrated in Fig. 2, the BTS/SS nanocomposites show slightly lower

electrical conductivities (565–430 S/cm) compared with the matrix BTS, due to the carrier scattering at BTS/SS interfaces. As the content of the SnS₂ nanosheets increasing, the electrical conductivities gradually decreased, which could be attributed to the increased density of BTS/SS interfaces. Corresponding to the electrical conductivities, the BTS/SS nanocomposites have greater increased $|S|$ (140–170 $\mu\text{V/K}$) compared to the BTS (110–130 $\mu\text{V/K}$) due to the introduction of barriers at BTS/SS interfaces. As a result of the moderate electrical conductivity and improved Seebeck coefficient, a high power factor about 1.40 $\text{mW m}^{-1} \text{K}^{-2}$ for BTS/SS2 is obtained, which show 30% enhancement compared with BTS (1.09 $\text{mW m}^{-1} \text{K}^{-2}$). It is noted that large efforts have been devoted to optimize the energy filtering of nanometer size potential barriers. For an optimized potential barriers design, the position of the Fermi level above the band edge should be large; the barrier height should be comparable to $k_{\text{B}}T$ and barrier width should be large enough to suppress tunneling, which could make 40% improvement in the power factor [31–33]. For BTS/SS nanocomposites, the barrier height at the BTS/SS interface (about 0.08 eV) and the barrier width (about 4 nm) were all fulfilled, which may be crucial to the enhancement of power factor. As expected, the constructed BTS/SS

interface could significantly reduce the thermal conductivity as illustrated in Fig. 2d. The κ_{total} is decreased with increasing SnS₂ volume fraction ($\kappa_{\text{total}} = 0.62 \text{ W m}^{-1} \text{ K}^{-1}$ is found for the BTS/SS3), mainly due to the decreasing of lattice thermal conductivity ($\kappa_{\text{latt}} = 0.39 \text{ W m}^{-1} \text{ K}^{-1}$ for the BTS/SS3). Due to the high power factor as well as low κ_{total} , a significantly enhanced ZT is expected in the BTS/SS sample (Fig. 2f). A high ZT = 0.79 is obtained for the BTS/SS3 at 423 K, which is nearly 180% higher than that of BTS (ZT = 0.49 at 423 K). Therefore, to construct the BTS/SS nanocomposites is a rational approach to optimize carrier and phonon transport characteristics by BTS/SS interface, which can be further regulated by varying the thickness of SnS₂ nanosheets.

Thus, the enhanced thermoelectric performance of BTS/SS nanocomposites could be attributed to the optimized carrier and phonon transport characteristics by BTS/SS interface. It would be interesting to investigate how the thickness of SnS₂ layers regulates the carrier and phonon transport characteristics of the BTS/SS nanocomposites. Therefore, SnS₂ nanosheets with different thickness have been synthesized and used to construct the BTS/SS nanocomposites (Fig. S7 and S8). The entire BTS/SS nanocomposites have the same SnS₂ nanosheets content (about 1.47 vol%), which is the optimum content for the SnS₂-t3 (about 4 nm) as discussed above. Compared to the BTS (728 S/cm at 300 K), the electrical conductivities of the BTS/SS nanocomposites with different thickness SnS₂ nanosheets (606–481 S/cm at 300 K) are reduced by 20 ~ 30% (Fig. 3a), due to the carrier scattering at the interfaces [34–37]. For the BTS/SS nanocomposites with different thickness SnS₂ nanosheets, the electrical conductivity decreases with decreasing the thickness of SnS₂ layers, which relate to the thickness of SnS₂ layers as well as the density of interfaces. It should be noted that the density of interfaces could increase with

decreasing SnS₂ nanosheets thickness, which is the main reason leading to decreasing of electrical conductivity. For the BTS/SS-t4, the density of interfaces is significantly higher than BTS/SS-t1 (about 7 times estimated by the nanosheet thickness), but the electrical conductivity is only reduced by about 20%, indicating that the SnS₂ layers at grain boundaries with thin thickness have minimal effect on electronic properties. Moreover, compared to BTS ($2.5 \times 10^{19} \text{ cm}^{-3}$), the carrier concentration of BTS/SS raised ($2.9\text{--}3.6 \times 10^{19} \text{ cm}^{-3}$), which may originate from the high density interfaces defect and distortions. Simultaneously, the carrier mobility decreases from 165 to $82 \text{ cm}^2/\text{Vs}$, results in the decreased electrical conductivity of BTS/SS nanocomposites. This decrease in mobility is due to carrier scattering arising from the high density interfaces. Meanwhile, the power factor is also increased with the decreased SnS₂ layers thickness, leading to that a high power factor about $1.45 \text{ mW m}^{-1} \text{ K}^{-2}$ of BTS/SS-t4 is obtained, which could be attributed to the low-energy electron-filtering effects at BTS/SS interfaces. For BTS/SS nanocomposites, the energy barrier at the BTS/SS interface is central to optimize the carrier transport characteristics. The band diagram of the BTS–SnS₂–BTS interface (Fig. 3c) reveals that an energy barrier with the height of $\Delta E = 0.08 \text{ eV}$ exists between the conduction band extremes of BTS and SnS₂ [38,39]. To maximize the power factor of the nanocomposites, the optimum potential barrier should be close to $k_B T$ (or somewhat higher) according to the previous theoretical study [31], which is fulfilled in the BTS/SS nanocomposites. For a single parabolic band and energy-independent carrier scattering approximation for degenerated semiconductors [38],

$$S = \frac{8\pi^2 k_B^2}{3eh^2} \left(\frac{\pi}{3n} \right)^{\frac{2}{3}} m_d^* T$$

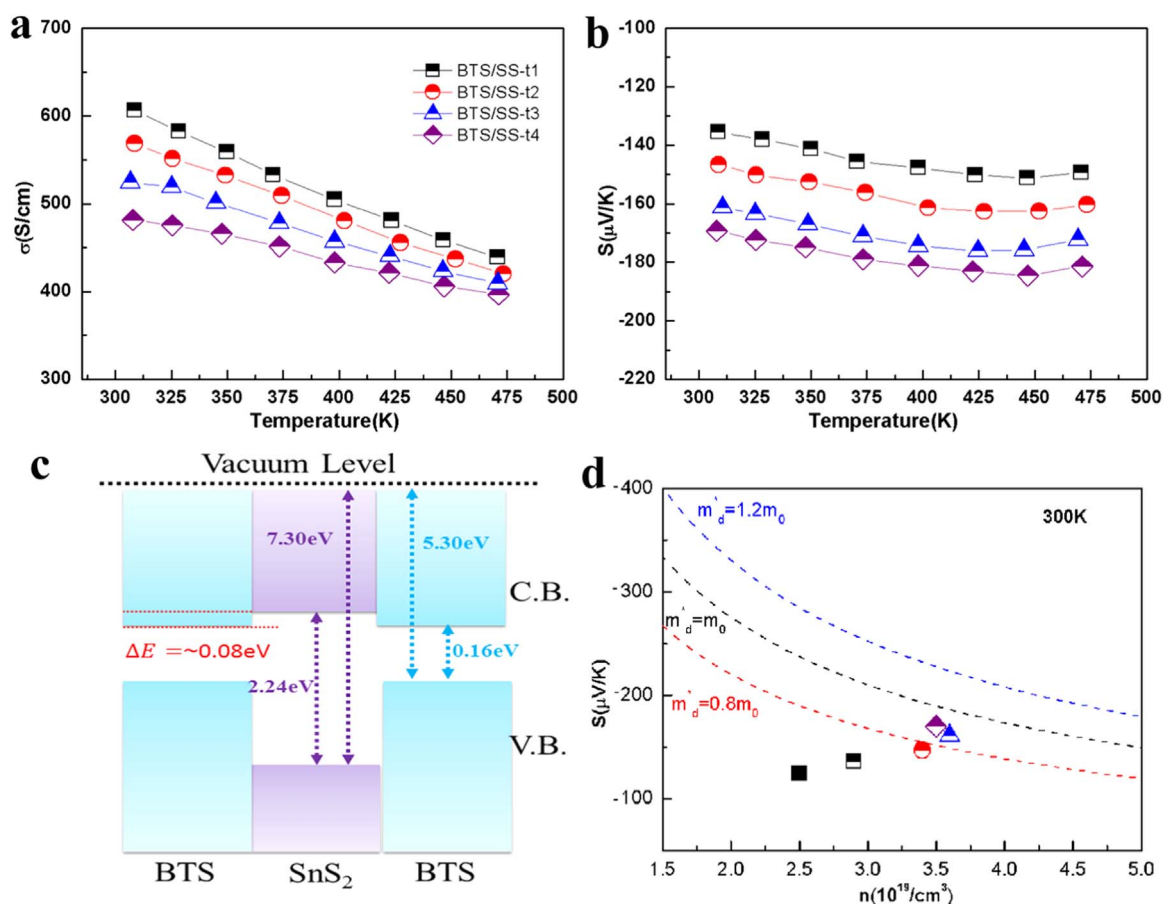


Fig. 3. The electrical transport properties of the BTS/SS nanocomposites with different thickness of SnS₂ nanosheet. (a) electrical conductivity (σ). (c) Band diagram of the BTS–SnS₂–BTS interface. (d) Seebeck coefficient (S) as a function of carrier concentration (n) for the BTS/SS nanocomposites.

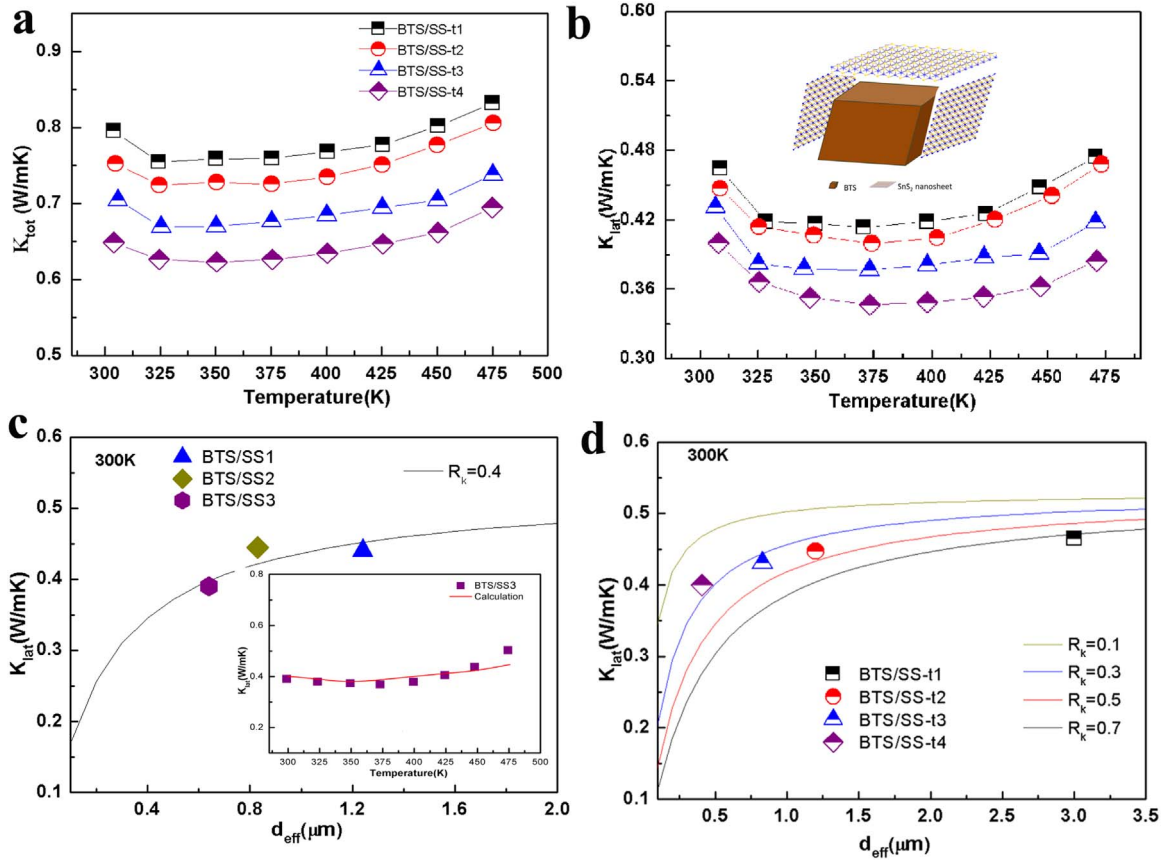


Fig. 4. (a) Temperature dependence of κ_{tot} for the BTS/SS nanocomposites with different thickness of SnS₂ nanosheet. (b) lattice thermal conductivity (κ_{latt}). (c) Room temperature lattice thermal conductivity with varying effective grain size (determined by the content of SnS₂, the inset is the κ_{latt} of BTS/SS3 compared with the calculated results from Eq. (1)). (d) Room temperature lattice thermal conductivity of BTS/SS nanocomposites with different thickness of SnS₂ nanosheet.

where m_d^* is the density of states (DOS) effective mass and k_B , e , and h are the Boltzmann constant, elementary charge, and the Planck constant, respectively. Thus, plot the Seebeck coefficient as a function of carrier concentration could clarify the electronic transport behavior in the BTS/SS nanocomposites, as shown in Fig. 3d. It is found that the m_d^* increases from 0.7 m_0 (BTS) to $\sim 1.0 m_0$ (BTS/SS-t4) by construct the BTS/SS nanocomposites, mainly due to the energy-filtering effect. Meanwhile, according to the theoretical study, tunneling carriers caused by the very thin barriers have negative effect on the Seebeck coefficient and power factor [38,40]. However, for the BTS/SS nanocomposites with different thickness SnS₂ nanosheets, the absolute value of Seebeck coefficient and the power factor increases with decreasing the thickness of SnS₂ layers, which means that the thickness of SnS₂ layers may be not thin enough for the carriers tunneling in the BTS/SS nanocomposites.

The total thermal conductivity of BTS/SS nanocomposites with different thickness SnS₂ nanosheets is shown in Fig. 4a. The total thermal conductivity (κ_{tot}) contains contributions from the electronic thermal conductivity (κ_{el}), lattice thermal conductivity (κ_{latt}), expressed as $\kappa_{tot} = \kappa_{el} + \kappa_{latt}$. The κ_{el} is estimated according to the Wiedemann-Franz law ($\kappa_{el} = L\sigma T$, L is the Lorentz number calculated using the Fermi integral function (S10)) [41]. Introduction of SnS₂ layer into the BTS grain boundaries significantly reduces the κ_{tot} , which has been conformed by all the BTS/SS nanocomposites. As the thickness of SnS₂ layers is decreased, the κ_{tot} is slightly decreased, which could be ascribed to the increasing density of the BTS/SS interface as well as the classical size effect, which suggests that the nanoscale interfaces impose strong boundary scatterings on phonons and suppress the thermal conductivity.

Based on previous research, a simple model for thermal conduction in the BTS/SS nanocomposites was constructed to understand the

effect of the BTS/SS interface [42,43]. In this model the interfacial thermal resistance contains contributions from the initial BTS matrix determined for the main materials and an additional contribution from the BTS/SS interface. It is well known that the thermal resistance from the BTS/SS interface is related to the interface density; here we use a simple model of cubic grains surrounded by the SnS₂ layers with edge length d_{eff} where the linear density of BTS/SS interfaces is the inverse of the equivalent average grain size, which is similar to the previous reports [44,45]. In this model, the d_{eff} determined by the volume fraction (V_f) and thickness (t) of SnS₂ nanosheets, expressed as, $t = d_{eff} \times V_f/3$ (Table S1). Then, the κ_{latt} of BTS/SS nanocomposites is fit to,

$$\kappa_{BTS/SS}^{-1} = \kappa_{BTS}^{-1} + R_k/d_{eff} \quad (1)$$

where the interfacial thermal resistance (for a unit area) R_k reflects the BTS/SS interface contribution for the reduce of the κ_{latt} . Thus, by plotting the κ_{latt} at 300 K of BTS/SS nanocomposites with different SnS₂ content (SnS₂-t3) as a function of d_{eff} , it is found that all the data agree well with the predicted curve calculated through the model with $R_k = 0.4 \times 10^2 \text{ m}^2 \text{ KW}^{-1}$, as shown in Fig. 4c. Meanwhile, the κ_{latt} for BTS/SS3 calculated in Eq. (1) with $R_k = 0.4 \times 10^2 \text{ m}^2 \text{ KW}^{-1}$ and corresponding d_{eff} (0.64 μ m) also agree well with the experimental values, which confirmed the effectiveness of the model. It is worth noting that at high temperature range, the value of κ_{latt} is slightly lower than the calculated curve, which could be ascribed to the contribution of bipolar diffusion. In contrast, for the BTS/SS nanocomposites with different thickness SnS₂ layer, the R_k is decrease from $0.7 \times 10^2 \text{ m}^2 \text{ KW}^{-1}$ to $0.1 \times 10^2 \text{ m}^2 \text{ KW}^{-1}$ with decreasing of SnS₂ layer thickness (Fig. 4d), which clearly reveals the modulation of thickness of SnS₂ layers at interfaces to the phonon transport. In conclusion, in present BTS/SS nanocomposites, as the decreasing of SnS₂ layer thickness, the interfacial thermal resistance is decreased, which might

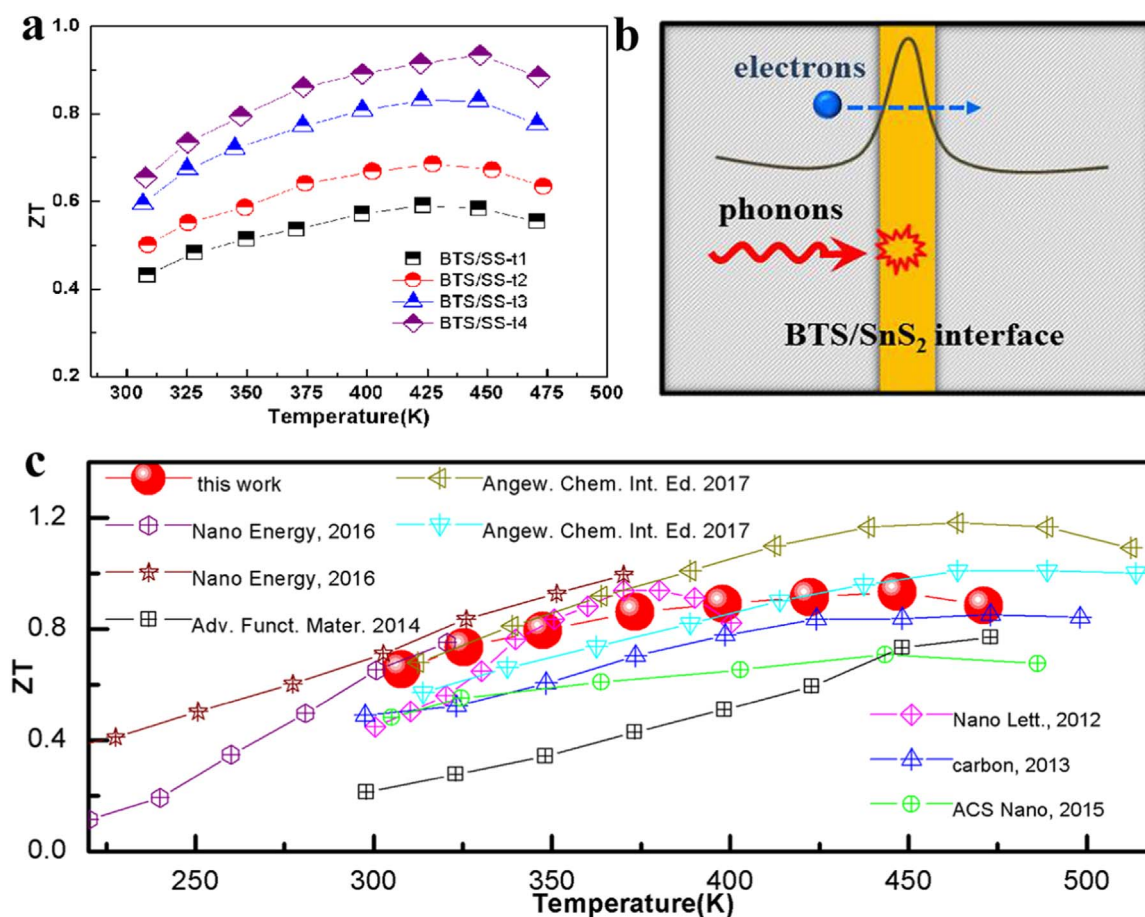


Fig. 5. (a) Thermoelectric figure of merit ZT of the BTS/SS nanocomposites with different thickness of SnS₂ nanosheet. (b) Mechanisms that contribute to the high ZT value of the n-type BTS/SS nanocomposites. (c) Comparison of the figure of merit ZT of this work with previous reported Bi₂Te₃-based nanomaterials.

mainly due to the size-dependent bipolar thermos-diffusion. It is well-known that the bipolar thermos-diffusion is very sensitive to the band structure of nanocomposites related to interface energy barrier [44]. Corresponding to the carrier transport, the size-dependent sharp transitions of states density could also affect the bipolar thermos-diffusion, which finally impact on the interfacial thermal resistance [36,45–46]. Accurate quantification of bipolar thermos-diffusion is difficult, which should be further explored. Despite the interfacial thermal resistance reduced with the thickness of SnS₂ layers decreasing, the κ_{tot} is still decreased due to the increased BTS/SS interface density.

Taking advantage of the enhanced power factor and maximum reduced κ_{tot} by regulated the SnS₂ layer thickness, the figure of merit ZT of the BTS/SS nanocomposites is further improved significantly, as shown in Fig. 5a. The maximum ZT value is 0.93 at 450 K for BTS/SS-t4, which is an excellent and highly competitive value compared to the best results of currently explored BT-nanostructures TE materials (Fig. 5b) [12,16,30,47–51]. Thus, these work give a glimpse of this viewpoint that the size-dependent effect could be used to optimal regulate the electrical conductivity (energy filtering effect) and phonon scattering (classical size effect), which finally give rise to the enhancement of ZT . We anticipate that further increase in thermoelectric performance could be realized by optimizing the energy barriers of heterojunction interface and controlling the defect type and density.

4. Conclusions

In summary, BTS/SS nanocomposites with a unique hetero-structure, in which the 2D atomically thin SnS₂ nanosheets (2–15 nm) are homogeneously assembled on BTS grain boundaries, have been

successfully synthesized, which exhibits an enhanced thermoelectric performance. The simultaneously optimization of electron and phonon transport is achieved. The enhanced Seebeck coefficient and power factor demonstrate that the carrier transport characteristics could be optimized by low-energy electron filtering effect, which could be adjusted by controlling the thickness of SnS₂ layers. Additionally, via a simple model, we systematic study the effect of the thickness of SnS₂ layers to the BTS-SnS₂-BTS interfaces thermal resistance, which show that size-dependent bipolar thermos-diffusion may be the dominant factors. Taking advantage of the unique structure as well as the optimal regulation to the thickness of BTS-SnS₂-BTS interfaces, a maximum ZT of 0.93 is obtained at 450 K for the BTS/SS-t4 ($t_4 = 2$ nm, about 1.47 vol%), approximately two times higher than that of the sample without SnS₂ layers. Thus, the strategy proposed in our work provides a route to design hybrid structures as well as explore the relationship between structure and properties for advanced TE materials.

Acknowledgment

The work was financially supported by National Materials Genome Project (2016YFB0700600), Shenzhen Science and Technology Research Grant (No. JCYJ20150629144612861), China Postdoctoral Science Foundation funded project (No.2016M600862).

Appendix A. Supplementary material

Supplementary data associated with this article can be found in the online version at doi:10.1016/j.nanoen.2017.07.011.

References

- [1] L.E. Bell, *Science* 321 (2008) 1457–1461.
- [2] M.G. Kanatzidis, *MRS Bull.* 40 (2015) 687–694.
- [3] B. Xu, M.T. Agne, T. Feng, T.C. Chasapis, X. Ruan, Y. Zhou, H. Zheng, J.-H. Bahk, M.G. Kanatzidis, G.J. Snyder, *Y. Wu, Adv. Mater.* 29 (10) (2017) 1605140–1605148.
- [4] L. Hu, H. Wu, T. Zhu, C. Fu, J. He, P. Ying, X. Zhao, *Adv. Energy Mater.* 5 (2015) 1500411–1500423.
- [5] S. Wang, Y. Sun, J. Yang, B. Duan, L. Wu, W. Zhang, J. Yang, *Energy Environ. Sci.* 9 (11) (2016) 3436–3447.
- [6] M. Hong, T.C. Chasapis, Z.-G. Chen, L. Yang, M.G. Kanatzidis, G.J. Snyder, J. Zou, *ACS Nano* 10 (4) (2016) 4719–4727.
- [7] T.-R. Wei, G. Tan, X. Zhang, C.-F. Wu, J.-F. Li, V.P. Dravid, G.J. Snyder, M.G. Kanatzidis, *J. Am. Chem. Soc.* 138 (28) (2016) 8875–8882.
- [8] K. Park, K. Ahn, J. Cha, S. Lee, S.I. Chae, S.-P. Cho, S. Ryee, J. Im, J. Lee, S.-D. Park, M.J. Han, I. Chung, T. Hyeon, *J. Am. Chem. Soc.* 138 (43) (2016) 14458–14468.
- [9] B. Liao, G. Chen, *MRS Bull.* 40 (2015) 746.
- [10] M.S. Dresselhaus, G. Chen, M.Y. Tang, R. Yang, H. Lee, D. Wang, Z. Ren, J.-P. Fleurial, P. Gogna, *Adv. Mater.* 19 (2007) 1043–1053.
- [11] H. Fang, Y. Wu, *J. Mater. Chem. A* 2 (2014) 6004–6014.
- [12] H. Yang, J.-H. Bahk, T. Day, A.M.S. Mohammed, G.J. Snyder, A. Shakouri, Y. Wu, *Nano Lett.* 15 (2) (2015) 1349–1355.
- [13] S. Li, T. Fan, X. Liu, F. Liu, H. Meng, Y. Liu, F. Pan, *ACS Appl. Mater. Interfaces* 9 (2017) 3677–3685.
- [14] G. Tan, F. Shi, S. Hao, H. Chi, L.-D. Zhao, C. Uher, C. Wolverton, V.P. Dravid, M.G. Kanatzidis, *J. Am. Chem. Soc.* 137 (2015) 5100–5112.
- [15] R.J. Mehta, Y. Zhang, C. Karthik, B. Singh, R.W. Siegel, T.B. Tasciuc, G. Ramanath, *Nat. Mater.* 11 (2012) 233–240.
- [16] Q. Zhang, X. Ai, L. Wang, Y. Chang, W. Luo, W. Jiang, L. Chen, *Adv. Funct. Mater.* 25 (6) (2015) 966–976.
- [17] G. Zhang, B. Kirk, L.A. Jauregui, H. Yang, X. Xu, Y.P. Chen, Y. Wu, *Nano Lett.* 12 (2012) 56–60.
- [18] Y. Sun, H. Cheng, S. Gao, Q. Liu, Z. Sun, C. Xiao, C. Wu, S. Wei, Y. Xie, *J. Am. Chem. Soc.* 134 (2012) 20294–20297.
- [19] M. Hong, Z.-G. Chen, L. Yang, G. Han, J. Zou, *Adv. Electron. Mater.* 1 (6) (2015) 1500025.
- [20] Y. Liu, C. Xiao, Z. Li, Y. Xie, *Adv. Energy Mater.* 6 (2016) 1600436.
- [21] S. Li, C. Xin, X. Liu, Y. Feng, Y. Liu, J. Zheng, F. Liu, Q. Huang, Y. Qiu, J. He, J. Luo, F. Pan, *Nano Energy* 30 (2016) 780–789.
- [22] E. Sutter, Y. Huang, H.-P. Komsa, M. Ghorbani-Asl, A.V. Krashennnikov, P. Sutter, *Nano Lett.* 16 (7) (2016) 4410–4416.
- [23] Y. Huang, E. Sutter, J.T. Sadowski, M. Cotlet, O.L.A. Monti, D.A. Racke, M.R. Neupane, D. Wickramaratne, R.K. Lake, B.A. Parkinson, P. Sutter, *ACS Nano* 8 (10) (2014) 10743–10755.
- [24] Y. Liu, H. Kang, L. Jiao, C. Chen, K. Cao, Y. Wang, H. Yuan, *Nanoscale* 7 (2015) 1325–1332.
- [25] A. Ambrosi, Z. Sofer, J. Luxa, M. Pumera, *ACS Nano* 10 (12) (2016) 11442–11448.
- [26] Y. Zhang, P. Zhu, L. Huang, J. Xie, S. Zhang, G. Cao, X. Zhao, *Adv. Funct. Mater.* 25 (3) (2015) 481–489.
- [27] Y.Q. Lei, S.Y. Song, W.Q. Fan, Y. Xing, H.J. Zhang, *J. Phys. Chem. C* 113 (2009) 1280–1285.
- [28] M. Hong, Z.G. Chen, L. Yang, J. Zou, *Nano Energy* 20 (2016) 144–155.
- [29] E. Lee, J. Ko, J.-Y. Kim, W.-S. Seo, S.-M. Choi, K.H. Lee, W. Shim, W. Lee, *J. Mater. Chem. C* 4 (2016) 1313–1319.
- [30] Y. Min, G. Park, B. Kim, A. Giri, J. Zeng, J.W. Roh, S. Il Kim, K.H. Lee, U. Jeong, *ACS Nano* 9 (7) (2015) 6843–6853.
- [31] N. Neophytou, H. Kosina, *J. Appl. Phys.* 114 (2013) 044315.
- [32] R. Kim, M.S. Lundstrom, *J. Appl. Phys.* 111 (2) (2012) 024508.
- [33] R. Kim, M.S. Lundstrom, *J. Appl. Phys.* 110 (2011) 034511.
- [34] P.K. Rawat, B. Paul, P. Banerji, *ACS Appl. Mater. Interfaces* 6 (2014) 3995–4004.
- [35] L.-D. Zhao, V.P. Dravid, M.G. Kanatzidis, *Energy Environ. Sci.* 7 (2014) 251–268.
- [36] W.-S. Liu, B.-P. Zhang, J.-F. Li, H.-L. Zhang, L.-D. Zhao, *J. Appl. Phys.* 102 (2007) 103717.
- [37] Y. Li, Y. Dou, X. Qin, J. Zhang, H. Xin, D. Li, C. Song, T. Zou, Y. Liu, C. Li, *RSC Adv.* 6 (2016) 12243.
- [38] E. Lee, J. Ko, J.-Y. Kim, W.-S. Seo, S.-M. Choi, K.H. Lee, W. Shime, W. Lee, *J. Mater. Chem. C* 4 (2016) 1313–1319.
- [39] L.A. Burton, D. Colombara, R.D. Abellon, F.C. Grozema, L.M. Peter, T.J. Savenije, G. Dennler, A. Walsh, *Chem. Mater.* 25 (2013) 4908–4916.
- [40] N. Neophytou, X. Zianni, H. Kosina, S. Frabboni, B. Lorenzi, D. Narducci, *Nanotechnology* 24 (2013) 205402.
- [41] W.-S. Liu, B.-P. Zhang, L.-D. Zhao, J.-F. Li, *Chem. Mater.* 20 (2008) 7526–7531.
- [42] B. Xu, M.T. Agne, T. Feng, T.C. Chasapis, X. Ruan, Y. Zhou, H. Zheng, J.-H. Bahk, M.G. Kanatzidis, G.J. Snyder, Y. Wu, *Adv. Mater.* 29 (2017) 1605140.
- [43] J. Amrit, *J. Phys. D: Appl. Phys.* 39 (2006) 4472–4477.
- [44] J.-H. Bahk, A. Shakouri, *Appl. Phys. Lett.* 105 (2014) 052106.
- [45] R. Yang, G. Chen, M.S. Dresselhaus, *Phys. Rev. B* 72 (2005) 125418.
- [46] P. Zong, R. Hanus, M. Dylla, Y. Tang, J. Liao, Q. Zhang, G.J. Snyder, L. Chen, *Energy Environ. Sci.* 10 (2017) 183–191.
- [47] P. Zong, X. Chen, Y. Zhu, Z. Liu, Y. Zeng, L. Chen, *J. Mater. Chem. A* 3 (2015) 8643.
- [48] B. Xu, T. Feng, M.T. Agne, L. Zhou, X. Ruan, G.J. Snyder, Y. Wu, *Angew. Chem.* 129 (2017) 3600–3605.
- [49] C. Zhang, M. Mata, Z. Li, F.J. Belarri, J. Arbiol, K.A. Khor, D. Poletti, B. Zhu, Q. Yan, Q. Xiong, *Nano Energy* 30 (2016) 630–638.
- [50] K.T. Kim, S.Y. Choi, E.H. Shin, K.S. Moon, H.Y. Koo, G.-G. Lee, G.H. Ha, *Carbon* 52 (2013) 541–549.
- [51] C. Zhou, C. Dun, K. Wang, X. Zhang, Z. Shi, G. Liu, C.A. Hewitt, G. Qiao, D.L. Carroll, *Nano Energy* 30 (2016) 709–716.



Dr. Shuankui Li received his Ph.D. degree in Condensed Matter Physics in 2014 from Lanzhou University, China. He is currently a post-doctoral fellow at School of Advanced Materials, Peking University, Shenzhen Graduate School with a research focus on design and preparation high performance nanostructured thermoelectric materials.



Xuerui Liu received his B.S. degree in Materials Chemistry from Peking University, China in 2015. He is pursuing his M.S. degree in the School of Advanced Materials, Peking University, China. His research interest is thermoelectric materials



Dr Yidong Liu is currently distinguished researcher in School of Advanced Materials, Peking University Shenzhen Graduate School. He received his Ph.D. in Chemistry from the Graduate Center/ CUNY in 2006. After his Ph.D., he moved to Columbia University as an associate research scientist. His research concentrates in high performance materials, composite and devices.



Fu-Sheng Liu received his Ph.D. in condensed matter physics in 2005 from Institute of Physics, Chinese Academy of Sciences (CAS), China. From 2005 to now, he joined in Shenzhen University as a full professor. His current research interests include crystal structure, metallic functional materials, thermoelectric materials and their related properties. He has authored and co-authored more than 100 refereed journal publications.



Professor Jun Luo received his Ph.D. in Condensed Matter Physics from the Institute of Physics, Chinese Academy of Science, in 2005. Then, he was awarded an Alexander von Humboldt Research Fellowship to visit Free University of Berlin. He went back to Institute of Physics, Chinese Academy of Science, in 2007, and worked there for 7 years. In October of 2013, he moved to Shanghai University and continued his work on thermoelectric materials.



Prof. Feng Pan, National 1000-plan Professor, Founding Dean of School of Advanced Materials, Peking University Shenzhen Graduate School, Director of National Center of Electric Vehicle Power Battery and Materials for International Research, got B.S. from Dept. Chemistry, Peking University in 1985 and PhD from Dept. of P & A Chemistry, University of Strathclyde, Glasgow, UK, with "Patrick D. Ritchie Prize" for the best Ph.D. in 1994. With more than a decade experience in large international incorporations, Prof. Pan has been engaged in fundamental research and product development of novel optoelectronic and energy storage materials and devices. As Chief Scientist, Prof. Pan led 8 entities in Shenzhen to win the

150 million RMB grant for the national new energy vehicles (power battery) innovation project from 2013 to end of 2015. As Chief Scientist, Prof. Pan led 12 entities to win

National Key project of Material Genomic Engineering for Solid State Li-ion Battery in China in 2016.